Characterization of Sea Surface Microlayer and Marine Aerosol Organic Composition using STXM-NEXAFS Microscopy and FTIR Spectroscopy

Savannah Lewis[1], Lynn M. Russell[1], Georges Saliba[2], Patricia K. Quinn[3], Timothy Bates[3, 4], Craig A. Carlson[5], Nicholas Baetge[6], Lihini Aluwihare[1], Emmanuel Boss[6], Nils Haentjens[6], Amanda Frossard[8], Tom Bell[9,10], and Michael Behrenfeld[6]

[1]Scripps Institution of Oceanography, University of California, San Diego, La Jolla, California, USA,
[2] California Air Resource Board, Sacramento, California, USA
[3] Pacific Marine Environmental Laboratory, NOAA, Seattle, Washington, USA
[4] Cooperative Institute for Climate, Oceans, and Ecosystem Studies (CICOES), University of Washington, Seattle, Washington, USA,
[5] Department of Ecology, Evolution and Marine Biology, University of California, Santa Barbara, CA, USA
[6] Department of Botany and Plant Pathology, Oregon State University, Corvallis, Oregon, USA
[7] School of Marine Sciences, University of Maine, Orono, ME, USA
[8] Department of Chemistry, University of Georgia, Athens, GA, USA
[9] Plymouth Marine Laboratory, Prospect Place, The Hoe, Plymouth, PL1 3DH, UK
[10] Department of Earth System Science, University of California, Irvine, CA, USA

Correspondence: Lynn M. Russell, lmrussell@ucsd.edu

Abstract

Atmospheric submicron particles, generated primary marine aerosol (gPMA), seawater (depth 5 m), and sea surface microlayer (depth ~0.001 m) samples were collected during the North Atlantic Aerosol and Marine Ecosystem Study (NAAMES) on the R/V *Atlantis* in September 2017 and March 2018 and analyzed by Scanning Transmission X-ray Microscopy with Near Edge X-Ray Absorption Fine Structure (STXM NEXAFS) and Fourier Transform Infrared spectroscopy (FTIR). Three organic functional groups (hydroxyl, alkane, and amine) were in all sample types, with the hydroxyl group typically being 50-90% of the quantified organic mass concentration. Microlayer and atmospheric particle samples both had a larger range of hydroxyl group to alkane group mass ratios than either seawater or gPMA. These data suggest that the sea surface microlayer organic composition contributes to the range of submicron atmospheric aerosol organic functional group composition. Atmospheric and microlayer sample alkane/hydroxyl group ratio variations were also associated with tracers of seawater biological activity, including chlorophyll and net primary production. Seawater and gPMA samples had relatively constant organic functional group composition for all of the sampled locations and varying phytoplankton activity conditions, suggesting they are associated with the more

invariant nature of dissolved organic carbon concentrations in seawater. Eight k-means clusters of STXM-NEXAFS particles were identified from the spectra for all four sample types (atmospheric aerosol particles, gPMA, seawater, and microlayer) and showed that all four sample types had particles in four to seven of the eight clusters included a mixture of sample types. These STXM-NEXAFS results support the FTIR measurements by showing consistent organic particle clusters across the four sample types.

Introduction

The microlayer has been proposed to be a significant source of organic material to the marine atmosphere because it separates the air-sea interface [*Cunliffe et al.*, 2013; *Engel et al.*, 2017], but there are few observations supporting this connection. The sea surface microlayer (SML) is operationally defined as the uppermost 1 – 1000 μm of the ocean [*Hunter and Liss*, 1977; *Liss*, 1997]. The SML is characterized by its enrichment of organic and inorganic components, including amino acids, proteins, and lipids, compared to sub-surface seawater. This enrichment is attributed to bubbles rising through the water column and scavenging organics that subsequently accumulate in the SML [*Aller et al.*, 2017; *Engel et al.*, 2017; *Tseng et al.*, 1992].

The SML plays a role in the enrichment of organic components of primary marine aerosol through the mechanism of bubbles bursting at the ocean surface. When the entrained bubbles reach the surface, seawater drains from the bubble film, leaving an organic rich film that, when it bursts, ejects small particles into the atmosphere [*Blanchard*, 1964; *Facchini et al.*, 2008]. The SML has a heterogeneous composition which can be comprised of organic carbon, amino acids, carbohydrates, and Transparent Exopolymer Particles (TEP) [*Engel and Galgani*, 2016; *Wurl and Holmes*, 2008]. The chemical properties of the SML, including concentrations of TEP, free amino acids, and phosphate, have been shown to be variable, with the standard deviation of some variables being greater than the average of measured values [*Reinthaler et al.*, 2008; *Zäncker et al.*, 2017].

For comparison, marine aerosol particles have been shown to be both homogeneous in terms of submicron organic functional group composition [*Frossard et al.*, 2014; *Russell et al.*, 2010] and heterogeneous in terms of variety of micron-sized particle types [*Hawkins and Russell*, 2010; *Saliba et al.*, 2021]. The consistency in organic composition and CCN activity of marine aerosol, defined as the aerosol present during clean marine conditions, has been shown across several open ocean regions of the Pacific and Atlantic Oceans [*Bates et al.*, 2020; *Frossard et al.*, 2014; *Quinn et al.*, 2014; *Russell et al.*, 2010]. Aerosol particles collected from Sea Sweep, a device that generates primary aerosol by bubbling seawater from 1 m below the sea surface, have shown that gPMA results in relatively consistent CCN activity and size-resolved mass fractions [*Bates et al.*, 2020; *Bates et al.*, 2012]. From these studies, it has been hypothesized that dissolved organic carbon (DOC) is the pool of carbon that has a greater

influence on gPMA composition than particulate organic carbon (POC), since dissolved organic matter is the largest ocean reservoir of reduced carbon [*Beaupré et al.*, 2019; *Carlson and Hansell*, 2015; *Hansell et al.*, 2009; *Lewis et al.*, 2021]. This hypothesis is consistent with the fact that DOC is relatively invariant in concentration in comparison to particulate organic carbon (POC) and is present in both the SML and sub-surface water [*Carlson and Hansell*, 2015; *Gasparovic et al.*, 2005; *van Pinxteren et al.*, 2017]. However, the few available measurements of organic composition for individual particles sampled from within the SML span a diverse range of types that might indicate a role for POC and the SML in influencing sea spray formation.

To understand what role the SML plays in the composition of submicron atmospheric aerosol, we collected and analyzed samples of the SML, atmospheric aerosol particles, subsurface seawater, and gPMA that were collected within four hours of each other. There are very few studies in which SML, seawater, and atmospheric aerosol particles have been sampled simultaneously to allow assessment of how SML composition transfers to atmospheric aerosol [*van Pinxteren et al.*, 2017]. SML samples (depth ~0.001 m), sub-surface seawater samples (depth 5 m), gPMA from Sea Sweep [*Bates et al.*, 2012] (depth of ~1 m), and atmospheric aerosol particles (height 18 m) collected in September 2017 and March 2018 during the North Atlantic Aerosol and Marine Ecosystem Study (NAAMES) [*Behrenfeld et al.*, 2019] were analyzed using both single particle microscopy from Scanning Transmission X-Ray Microscopy with Near Edge X-Ray Absorption Fine Structure (STXM-NEXAFS) and FTIR. This study investigates this unique dataset to assess the degree to which SML and seawater have similar organic composition to gPMA and atmospheric aerosol particles.

Methods

NAAMES

NAAMES was an interdisciplinary investigation conducted to improve understanding of Earth's ocean-aerosol-cloud system [*Behrenfeld et al.*, 2019]. The campaign consisted of four cruises on the R/V *Atlantis* in the North Atlantic that each included 26 days at sea in November 2015 (NAAMES 1, Winter), May-June 2016 (NAAMES 2, Late Spring), September 2017 (NAAMES 3, Autumn), and March-April 2018 (NAAMES 4, Early Spring). The ship traveled to and from Woods Hole, MA, to ~ 55°N for the first three cruises. For NAAMES 4, the ship departed from San Juan, Puerto Rico, to ~44.5°N and returned to Woods Hole, MA. During each cruise, the ship occupied five to seven multi-day sampling stations to conduct biological and oceanographic experiments. SML samples were only collected on NAAMES 3 and NAAMES 4, so those are the only data used in this study.

Sea Sweep

The Sea Sweep is a primary marine aerosol particle generator that has been used to provide a surrogate for particles formed from bubble bursting at the ocean surface to investigate the properties of primary marine aerosol [*Bates et al.*, 2012]. Sea Sweep consists of

a stainless-steel frame attached to two inflatable pontoon floats and was deployed off the port bow of the R/V *Atlantis*. The sea surface inside the sampling hood is contained to capture aerosols produced from the microlayer, but splashing in high-wave conditions may modify the microlayer. The stainless-steel hood on top of the frame maintains a laminar flow air curtain of particle-free air (charcoal and HEPA filtered) at the bow and stern ends of the frame (Bates et al., 2012). Stainless steel frits, 200 µm in size, were positioned below the sea surface at approximately 0.75 m. The resulting particles were then transported to the instruments for analysis. Because the particles are transported directly to sampling instrumentation without time for atmospheric processes, they provide a convenient proxy for the "primary" component of sea spray aerosol.

Atmospheric Particle and gPMA Filter Collection

Atmospheric and gPMA particles were collected through a temperature-and humidity-controlled inlet during NAAMES. Atmospheric and generated primary marine aerosol (gPMA) particles were dried using diffusion driers filled with silica gel and collected on 37 mm Teflon filters (Pall Inc., 1 µm pore size) for FTIR spectroscopy analyses. < 1 µm filters for atmospheric and gPMA were sampled at 8.3 L min^{-1} after a <1 µm cyclone (SCC 2.229) at a flow rate of 16.7 L min^{-1}. Filters for <0.18 and <0.5 µm atmospheric and <1.1 µm gPMA particles were sampled at 10 L min^{-1} after Berner impactors sampling at 30 L min^{-1}. Filters were collected for 12-23 hours for atmospheric particle samples (<0.18, <0.5, and <1 µm) and two hours for Sea Sweep samples (<0.18, <1, and <1.1 µm), resulting in filtered air volumes of 1-13.8 m^{-3}. After collection, the filters were immediately unloaded, stored in petri dishes, and frozen at 0°C for later analysis at Scripps Institution of Oceanography.

Seawater and Microlayer Collection

Seawater and sea surface microlayer (SML) samples were collected during the NAAMES 3 (September 2017) and NAAMES 4 (March-April 2018) cruises when on station, which is described in Behrenfeld et al. [2019]. Six SML samples were chosen for further investigation: four from NAAMES 3 (09/10/17, 09/12/17, 09/15/17, and 09/16/17) and two from NAAMES 4 (03/27/18 and 04/03/18) (Table 1). These six SML samples were chosen because they had a start time within four hours of gPMA and atmospheric particle filter start times. The SML samples were collected via a Garrett screen [*Garrett*, 1967] (57.5 cm^2), which was attached to a nylon rope and lowered over the starboard side of the ship until it touched the surface of the ocean while horizontal and then pulled back up to the deck. The screen was then held at an angle to allow the SML sample to drain off the screen for approximately 1 minute, through an acid-cleaned glass funnel, and into an acid-cleaned polycarbonate bottle following the procedures used in prior studies [*Cunliffe and Wurl*, 2014]. This process was repeated until approximately 1.5 L was collected. Nitrile gloves were used whenever the Garrett screen was handled before and during sampling. The screen was rinsed with seawater between samples. The seawater samples were collected the same hour as the SML samples either using the ship in-line near-surface sampling system (NAAMES 3) or from 5-m CTD mounted Niskin bottles (NAAMES 4). The Imaging FlowCytobot (IFCB) cell biovolume was measured for the SML samples as well as for the in-line and Niskin seawater samples [*Chase et al.*, 2020; *Moberg and*

Sosik, 2012]. After SML collection, ~60 mL of seawater and SML samples were poured into amber storage bottles and immediately frozen at -20^{o} C to be later processed and analyzed for FTIR and STXM-NEXAFS analysis at Scripps Institution of Oceanography.

FTIR Spectroscopy and Algorithm

Samples on Teflon filters were analyzed using FTIR spectroscopy (Bruker Tensor 27 spectrometer with a deuterated triglycine sulfate, DTGS, detector) to measure the infrared transmission using 2 cm^{-1} resolution [*Takahama et al.*, 2013]. FTIR spectra were checked for hydrate absorption, and no samples had an identifiable amount so dehydration was not required [*Frossard and Russell*, 2012]. The FTIR spectrum for each filter was analyzed using an automated fitting algorithm [*Maria et al.*, 2002; *Russell et al.*, 2009b; *Takahama et al.*, 2013]. When the baselining procedure resulted in degenerate spectra, defined as spectra that have no discernable peaks and low signal to noise, they were excluded from further analysis. In this dataset, no filters had degenerate spectra. The FTIR spectrum for each filter was analyzed using an automated fitting algorithm [*Maria et al.*, 2002; *Russell et al.*, 2009b; *Takahama et al.*, 2013]. Five organic functional groups were quantified from these mixtures (alkane, hydroxyl, amine, carboxylic acid, and non-acidic carbonyl) and summed together to quantify the organic mass (OM) concentration, with groups below detection limit excluded.

OM group concentrations were considered above detection if they met three criteria: 1) the fitted peak area for the individual functional group exceeded the minimum observable peak area (defined below), 2) the fitted peak area for the individual functional group exceeded twice the standard deviation of the pre-scan background area, and 3) the alkane functional group was one of the groups that met the first two criteria [*Lewis et al.*, 2021]. OM from this technique has an uncertainty of ± 20% due to functional groups that overlapped the Teflon absorption, unquantified functional groups, and semi-volatile properties [*Maria et al.*, 2002; *Russell*, 2003; *Russell et al.*, 2009a; *Russell et al.*, 2009b; *Takahama et al.*, 2013].

Net Primary Production and Chlorophyll Measurements

Net Primary Production (NPP) (µmol C L^{-1} d^{-1}) was estimated using the Photoacclimation Productivity Model from Fox et al. [2020], which showed strong agreement with available measurements from 24 hour ^{14}C sodium bicarbonate uptake incubations. Shipboard chlorophyll concentrations were analyzed by a Wetlabs ACS which measured hyperspectral particulate attenuation and absorption, which are optical measurements commonly used to estimate chlorophyll concentration, calibrated to the NAAMES campaign [*Boss et al.*, 2001; *Cetinić et al.*, 2012]. NPP was normalized to the integrated depth of the euphotic zone for each station to obtain a consistent metric for the maximum column productivity. The column maximum was used since the bubble entrainment depth is not known and the mixing layer depth was variable (6-231 m during the NAAMES campaigns).

Sample Preparation

Frozen seawater and SML samples were brought to room temperature, atomized, dried using diffusion driers filled with silica gel, and collected on silicon nitride windows (Si_3N_4; Silson

Ltd.) mounted on a rotating impactor (Streaker; PIXE International, Inc.) at 1 LPM. The sampling times ranged from 3 to 5 min. Windows were frozen directly after collection and stayed frozen until time of analysis (samples were analyzed between September 2019 and June 2021). The seawater and SML samples were atomized with a constant output atomizer (TSI Model 3076) to prepare both filters for FTIR and silicon nitride windows for STXM-NEXAFS. The size distribution was not measured during this process, but the particles collected after drying are expected to be smaller than 1 µm based on the design.

Atmospheric particles and gPMA were collected on Teflon filters that were used directly for nondestructive FTIR spectroscopy. After FTIR was completed, the particles on each filter were extracted and dried on silicon nitride windows in order to compare the composition by STXM-NEXAFS [*Crilley et al.*, 2013]. To extract the particles from the filters, the filters were placed in a fume hood on isopropanol cleaned aluminum foil and 200 µL of HPLC-grade DI water (Sigma Aldrich) was aliquoted onto the center of the filter and agitated for 2 min. 20 µL from the filter were transferred to the silicon nitride windows and left to dry overnight. The samples were frozen at 0˚C until analysis. The particles that formed after the extracts collected on these samples dried ranged from 0.2 to 7.5 µm diameter.

Organic Functional Group Composition by STXM-NEXAFS

In all, 34 samples of extracted atmospheric particles, atomized SML, extracted gPMA, and atomized seawater from NAAMES 3 (September 2017) and NAAMES 4 (March 2018) were analyzed at the Advanced Light Source at Lawrence Berkeley National Laboratories Beamline 5.3.2.2 in a He-filled chamber using scanning transmission X-ray microscopy (STXM) with near edge X-ray absorption fine structure (NEXAFS) following established protocols [*Maria et al.*, 2004; *Russell et al.*, 2002]. These 34 samples resulted in 219 stacks of spectra from particles that ranged in size from 0.2 to 7.5 µm, where these sizes reflect the extracted or atomized sizes rather than their innate characteristics (and hence are not discussed here). These spectra were analyzed by an automated-shape recognition algorithm, which identified areas of high pre-edge density (non-carbon components) and high carbon density (post-edge minus pre-edge) [*Takahama et al.*, 2010]. Of these 219 particles stacks, 122 (56%) particles passed the quality control checks, including having carbon absorbance sufficiently above the noise. The 122 particles were then clustered into eight categories using the MATLAB k-means clustering algorithm.

Results

In this section, we report the differences in functional group composition for the different sample types (seawater, gPMA, SML, and atmospheric particle) and describe individual days on which multiple sample types were collected within four hours of each other.

Comparison of Different Sample Types

The four sample types (seawater, SML, gPMA, and atmospheric particle) show generally similar functional group composition by FTIR and STXM-NEXAFS, although indicators of small differences in molecular structures are present (Figures 1 and 2, respectively).

FTIR (Figure 1) and STXM-NEXAFS (Figure 2) spectra for seawater were similar during the three days that were sampled and above detection limit. All samples had high cosine similarity values with low standard deviations of 0.98 ± 0.02 (N=3) for FTIR and 0.97 ± 0.02 (N=7) for STXM-NEXAFS (Table 2). Seawater typically had an FTIR spectra with two hydroxyl group peaks, a broad alkane group peak at 2927 cm^{-1}, and a narrow amine group peak at 1615 cm^{-1} (Figure 1). The hydroxyl group fraction was 65-75% of the OM, followed by alkane group (15-25%) and amine group (<10%). The STXM-NEXAFS spectra show an aromatic/alkene carbon peak, alkyl carbon peak, and a small carboxylic acid carbon peak, with about one in three also having potassium peaks. The carboxylic acid group was below detection limit for FTIR, as is expected for seawater [*Frossard et al.*, 2014], but STXM-NEXAFS is a more sensitive instrument and carboxylic acids are a trace component of seawater composition [*Gagosian and Stuermer*, 1977]. STXM-NEXAFS shows four different k-means clusters of spectra for the seawater sample type.

Similar to previous studies [*Bates et al.*, 2012; *Frossard et al.*, 2014], gPMA FTIR spectra showed a high cosine similarity value with a low standard deviation (0.94 ± 0.06, N=4) between different days and two seasons, with hydroxyl groups having the highest group mass concentration, followed by alkane and amine functional groups (Figure 1). The STXM-NEXAFS spectra show carboxylic acid carbon, carbonate, and potassium peaks in four out of six of the samples and aromatic/alkene carbon peaks in half of the samples (Figure 2). The STXM-NEXAFS spectra were also similar to each other with a cosine similarity value of 0.97 ± 0.02 (N=19). There were six different k-means clusters of spectra for the gPMA sample type, showing a variety of individual particle compositions.

The SML FTIR spectra show the most variability, as demonstrated by the lowest cosine similarity value and highest standard deviation of the different sample types (0.72 ± 0.18, N=6). The different peak shapes and locations in the FTIR spectra vary from sample to sample (Figure 1, top right panel). However, FTIR-based organic functional group composition showed that the OM in the SML samples predominately consisted of the hydroxyl group (50 – 80%), followed by smaller mass contributions of alkane and amine functional groups (5 – 35%) (Figure 3). STXM-NEXAFS had a cosine similarity of 0.98 ± 0.02 (N=38). STXM-NEXAFS shows six different k-means clusters of spectra for the SML sample type, illustrating that the individual particle components are variable.

Two of six atmospheric particle FTIR spectra and all six STXM-NEXAFS spectra had carboxylic acid groups that were likely from secondary photo-oxidative processing. The presence of carboxylic acid groups is consistent with previous observations of ambient marine aerosol samples in clean conditions [*Frossard et al.*, 2014; *Russell et al.*, 2010;*Saliba et al.*, 2020]. While the FTIR hydroxyl group fraction varied from 50 to 90%,of the measured OM, there was no statistical difference ($p>0.05$) when the fractions of hydroxyl, alkane, and amine groups from the different sources were compared. Atmospheric particle samples had the second lowest FTIR cosine similarity value (0.75 ± 0.15, N=6) and the lowest STXM-NEXAFS

cosine similarity value (0.95 ± 0.1, N=58). All six centroids of STXM-NEXAFS spectra had an aromatic/alkene carbon peak, a carboxylic acid carbon peak, and a carbonate peak. Four of the six STXM-NEXAFS spectra also had an alkyl carbon peak and potassium peaks. All eight of the k-means clusters were found in the atmospheric particle sample type, making it the only sample type that contains every cluster.

Comparison of Sampled Days

Six sets of samples that were each collected on the same day were used to investigate connections between the four sample types (subsurface seawater, SML, gPMA, atmospheric aerosol) (Figure 4). This comparison was investigated to identify if there was a chemical signature that linked subsurface seawater and SML as sources for the gPMA or atmospheric particles.

The first set of samples analyzed from NAAMES 3 was on 10 September 2017 (Figure 4, row A), when there were three sample types: SML, gPMA, and atmospheric particles. The STXM-NEXAFS atmospheric particle and SML spectra both had an aromatic/alkene carbon peak, carboxylic acid carbon peak, and carbonate peaks. The gPMA spectrum also had a sharp alkyl carbon peak and carbonate peak.

Sampling on 12 September 2017 (Figure 4, row B) included all four sample types. STXM-NEXAFS showed that all four types have an aromatic/alkene carbon peak, and the gPMA, atmospheric particle, and sea water samples had a carbonate carbon peak. The FTIR showed the hydroxyl group peaks having nearly identical peak locations between 3338 and 3395 cm^{-1}. All four FTIR spectra had hydroxyl, alkane, and amine group peaks.

On 15 September 2017 (Figure 4, row C), three sample types were collected and analyzed (SML, gPMA and atmospheric particle), with each corresponding STXM-NEXAFS spectrum showing a carboxylic acid carbon peak, carbonate carbon peak, and potassium peaks. The atmospheric particle sample did not have an aromatic/alkene carbon peak, which was different than on 10 and 12 September 2017. The FTIR spectra from the three sample types were noticeably different from each other, with the atmospheric aerosol particle spectrum having an alkane group fraction that was twice as high as in the SML and seawater samples, as well as a large carboxylic acid group peak. The gPMA FTIR spectrum was similar to those from 10 and 12 September 2017. The SML FTIR spectrum had a similar hydroxyl group peak shape, but a larger amine group contribution than on 10 and 12 September 2017.

On 16 September 2017 (Figure 4, row D), the ship continued sampling at the same location as on 15 September 2017 and there were two types collected and analyzed: SML and atmospheric particle. The atmospheric particle sample had a STXM-NEXAFS spectrum with alkyl carbon peak, carboxylic acid carbon peak, and carbonate peaks, as well as an aromatic/alkene carbon peak. The FTIR spectrum showed a broader hydroxyl group peak and larger alkane group peaks in the atmospheric particle sample than in the SML sample. Compared to 15 September 2017, the SML FTIR spectrum had a larger alkane group contribution.

The first set of samples analyzed from NAAMES 4 was 27 March 2018 (Figure 4, row E), when there were three sample types: SML, seawater, and atmospheric particle. STXM-NEXAFS spectra showed that all three types have aromatic/alkene and carboxylic acid carbon peaks. The FTIR spectra showed that the three samples have similar hydroxyl group peak locations, with overlapping primary peaks between 3350 and 3370 cm^{-1}. The SML sample has a partial peak at 3510 cm^{-1} that is in three of the six SML samples in Figure 4. The atmospheric particle FTIR spectrum had sharp alkane group peaks, while the seawater had broad alkane group peaks and the SML had very little alkane group absorption.

On 3 April 2018 (Figure 4, row F), all four sample types were collected and analyzed. STXM NEXAFS spectra show a varied functional group composition, in which the seawater only had an aromatic/alkene carbon peak. The SML sample STXM-NEXAFS spectrum had an aromatic/alkene carbon peak, alkyl carbon peak, carboxylic acid carbon peak, carbonate peak, and potassium peaks. The gPMA sample has a carboxylic acid carbon peak, carbonate peak, and potassium peaks. The atmospheric aerosol particles STXM spectrum had aromatic/alkene carbon, carboxylic acid carbon, and carbonate peaks. The FTIR spectra displayed two main composition types, where SML and atmospheric particle types had narrower hydroxyl group peaks that are smaller than the broad alkane group peak. gPMA and seawater spectra showed a broad hydroxyl group peak with smaller and narrower alkane group peaks.

Seawater and gPMA (<1 and <1.1 μm) samples (blue and orange in Figure 4) show FTIR spectra that do not show much variation in composition (cosine similarity of 0.94 ± 0.06 and 0.98 ± 0.02) throughout the six days of sampling, with two hydroxyl group peaks comprising most of the OM, followed by broad alkane group absorption and an amine group absorption. STXM-NEXAFS spectra consistently (five of six) had aromatic/alkene and alkyl carbon peaks and occasionally (three of six) had carbonate and potassium absorption peaks. Atmospheric and SML samples (red and brown in Figure 4) showed far more variability in their FTIR spectra throughout the six days, as demonstrated by the high standard deviation in cosine similarity (0.75 ± 0.15 and 0.72 ± 0.18). The FTIR spectra showed more variation than STXM-NEXAFS spectra, as indicated by cosine similarity values lower than 0.8 (Table 2). STXM-NEXAFS showed that the majority (11 of 12) of atmospheric particle and SML spectra had an aromatic/alkene carbon peak and carboxylic acid carbon peak. All six atmospheric particle filters also had carbonate peaks, whereas only two of six SML samples had carbonate. The atmospheric particle filters were the most dissimilar of the four sample types using STXM-NEXAFS (0.95 ± 0.1).

FTIR spectra had lower cosine similarity values than NEXAFS spectra (Table 2), with hydroxyl, alkane, and amine groups being present in all samples and hydroxyl group accounting for 50 – 90% of the quantified OM. Seawater and gPMA samples had similar composition with hydroxyl groups comprising 70-90% of the quantified OM, with the remainder from alkane groups (5-20%) and amine groups (2-20%), throughout the sampling days which span two different seasons. The SML and atmospheric particle samples had FTIR spectra that were more

variable, but still included the same three organic functional groups (hydroxyl, alkane, and amine) and the hydroxyl group accounted for 40 - 80% of quantified OM.

The variability in the SML and atmospheric particle spectra were compared using the alkane-to-hydroxyl functional group ratio and several biological proxies, including in-line chlorophyll and net primary production (NPP) (Figure 5 and Figure S1). The alkane-to-hydroxyl group ratios had small ranges of alkane-to-hydroxyl group ratio, as evidenced by small standard deviations, for both seawater (0.08 ± 0.04) and gPMA (0.26 ± 0.08). SML and atmospheric particle alkane-to-hydroxyl group ratios showed more variability, with 0.37 ± 0.42 for SML and 0.5 ± 0.37 for atmospheric particles. Here, we found weak and moderate correlations between the alkane-to-hydroxyl group ratio and both in-line chlorophyll (Figure S1) and NPP (Figure 5) for both atmospheric particle (with no significance, $p = 0.24$) and SML samples (with no significance, $p = 0.12$) over a range of alkane to hydroxyl ratios from 0 to 1 (0.5 ± 0.4 and 0.4 ± 0.4, respectively). For seawater, there was no correlation, and the range of alkane to hydroxyl ratios were 0.2 ± 0.1. For gPMA, there was a strong negative correlation (with no significance, $p = 0.14$), but again low values and little variation in alkane to hydroxyl ratio 0.1 ± 0.01. While the sample size is too small to establish statistical significance of the correlations, the difference in the ranges of values is noteworthy with atmospheric particle and SML ranges 2-10 times greater than seawater and gPMA ranges. The in-line chlorophyll had similar correlations to that of NPP for atmospheric particle and SML alkane-to-hydroxyl group ratios.

Clusters of STXM-NEXAFS Spectra for Sampled Particles

The average spectra of 122 particles were clustered into eight spectra categories (Figures 6 and 7). Five of the spectra categories are similar enough to previously reported categories presented by Takahama *et al.,*[2007] that they are considered to be the same category (Figure 6 and Table 3). These five categories represented particles that were previously named d, g, j, l, and m and associated with combustion (g,m), freshly emitted black carbon (d), humic-like biogenic sources (g,j,m), and unidentified (l). Two other categories, Macid and Mcarb, were similar to particles identified as from ocean sea spray sources over the Southern Ocean, reported in Saliba et al [2021].

Particle spectra in cluster m had absorption in the aromatic/alkene, ketonic carbonyl, and alkyl carbon regions, similar to cluster m particles from Takahama et al., [2007] (cosine similarity = 0.99, two common peaks, Table 3). This cluster has particles from all four sample types (seawater, SML, gPMA, and atmospheric particle). The majority of SML particles (13 of 34) were in this cluster, which could mean that aromatic or alkene-containing substances such as phenols or humic materials are the source of the aromatic/alkene carbon peak [*Carlson and Mayer*, 1980; *Knulst et al.*, 1998]. It is also possible the aromatic/alkene carbon signal is from black carbon that had been deposited onto the sea surface or dissolved into the water column [*Bao et al.*, 2017]. The particles had a high carbon content and were mostly spherical, although it is prudent to recall that particle shape for atmospheric particle and gPMA filters represents the morphology of the dried extract rather than airborne particle morphology.

Particle spectra in cluster j had absorption in the aromatic/alkene carbon, carboxylic carbonyl carbon, carbonate, and potassium regions. This cluster was similar to Type j particles identified by *Takahama et al., [2007]* with a cosine similarity value of 0.94 and four common peaks (Table 3). This cluster had the second highest number of spectra with 24 out of 122 particles, including 13 SML, four gPMA, and seven atmospheric particles. Cluster j had the highest amount of SML particles. The morphology was a mixture of inorganic cores with organic coatings and clumps of organic-containing particles, indicating a likely marine biogenic source. Prior association of this type with humic and fulvic acids, soil substances, and biomass combustion by *Takahama et al., [2007]* suggests complex organic substances that may be surface active [*Hayase and Tsubota*, 1983] and have been measured previously in the SML [*Drozdowska et al.*, 2017].

Particle spectra in cluster Typed (cosine similarity 0.99, one common peak) have absorbance in the aromatic/alkene carbon region and small absorbance in the ketonic carbonyl carbon region. This cluster was present during both NAAMES 3 and NAAMES 4. This cluster had 17 out of 122 particles, including four SML, three gPMA, and 10 atmospheric particle samples. The lack of peaks in this cluster other than the aromatic/alkene carbon absorption indicates it is likely fresh black carbon [*Takahama et al.*, 2007]

Particle spectra in cluster Macid (cosine similarity 0.99, four common peaks, Table 3) were identified over the Eastern Pacific and over the Southern Ocean [*Laskin et al.*, 2012; *Saliba et al.*, 2021]. This cluster is in NAAMES 3 and NAAMES 4 as well, along with carboxylic carbonyl carbon, carbonate carbon, and potassium peaks. This cluster had the highest number of spectra with 25 particles from all four of the sample types. The morphology typically included low organic cuboidal shapes coated by organics, which likely represents a salt core with an organic coating [*Russell et al.*, 2010]. The acidic groups in the atmospheric particle samples may indicate that secondary photochemical processes have occurred.

Particles in cluster l had a clear absorption in the aromatic/alkene carbon region and a broader absorption in the ketonic carbonyl carbon region. These particles were similar to type l identified by Takahama et al., [2007] (cosine similarity = 0.99, two common peaks, Table 3), which was classified as not having an identified source because of the limited number of particles found and the limited availability of tracers for some types of sources. This cluster was present during both NAAMES 3 and NAAMES 4. This cluster had 10 out of 122 particles, including seven SML, one atmospheric, and two seawater particles.

Particles in cluster Mcarb accounted for 21 out of 122 particles and mostly consisted of extracted atmospheric particle particles, which are 17 out of the 21 particles. This cluster was present during both NAAMES 3 and NAAMES 4. This cluster was first observed in Saliba et al., [2021]. The cluster spectra include three peaks, namely alkyl carbon, carbonate, and potassium, and the spectra in the cluster have a cosine similarity of 0.98. This cluster is also similar to the calcareous phytoplankton cluster found in Hawkins and Russell, [2010]. However, the morphology of the particles from this campaign often had salt cores and diverse morphologies, whereas the calcareous phytoplankton type had structures that resembled cell or shell parts

without salt cores. This particle type was likely sea spray particles, but it included only particles that were extracted from filters (atmospheric particle and gPMA) for which the extracted morphology may be different from their airborne state.

Particles in cluster g included all four sample types and contained nine out of 122 particles from both campaigns. This particle type was previously identified [*Takahama et al.*, 2007] (cosine similarity = 0.96, two shared peaks, Table 3), and the particle cluster was identified as a combustion-related due to the prominent aromatic/alkene carbon peak and amorphous carboxylic carbonyl carbon absorption. The high carbon content and lack of potassium or alkyl groups in this cluster makes it likely that the cluster g particles in NAAMES 3 and NAAMES 4 are from combustion sources.

Particle spectra in cluster Csalt (crystallized salt) only accounted for three out of 122 particles and were from a single extracted atmospheric particle sample from NAAMES 3. This cluster is distinguished by the peak splitting at the two potassium peaks (297.4 and 299.9 eV). This may be due to the extracted particles crystalizing onto the silicon nitride windows, which has been shown to cause ligand field splitting [*Vedrinskii et al.*, 1982].

Discussion

Prior work has indicated the SML to be enriched in amino acids, lipids, and organics in comparison to subsurface seawater [*Aller et al.*, 2005; *Engel et al.*, 2017; *Obernosterer et al.*, 2008], suggesting that there would be a distinct difference in organic composition between the SML and the other sample types (seawater, gPMA, and atmospheric particles). SML and atmospheric particle samples are different from the seawater and gPMA samples as evidenced by their lower cosine similarity values for FTIR and higher standard deviations between cosine similarity values of individual FTIR spectra within the same sample type (Table 2, Figures 1 and 2). However, we see many similarities in composition between the four types of samples with both FTIR and STXM-NEXAFS. All have three organic functional groups (hydroxyl, alkane, and amine) with hydroxyl consistently being the largest fraction (Figures 1 and 3). Most particles sampled have an aromatic/alkene carbon peak in STXM-NEXAFS spectra, regardless of sample source (Figure 2). Both FTIR and STXM-NEXAFS show hydroxyl groups and alkane groups; alkene groups are present in the STXM-NEXAFS spectra for the four sample types, although they are below the detection limit for FTIR quantification (Figure 4). Seawater and gPMA samples had very consistent FTIR spectra across the sampled days with high cosine similarity values for spectra from the same sample type (Table 2). When the STXM-NEXAFS particles were separated into categories via k-means clustering, the only cluster that had particles from a single sample type was Csalt, which had only three atmospheric aerosol particles. Other than this new category (which may be associated with a salt artifact), there were no unique particle clusters that were from only one sample source, rather the particle clusters had particles from most of the sample sources.

While the FTIR organic functional group composition was similar on average for the four sample types, the FTIR spectra showed peaks at different locations and with different shapes, particularly in the alkane region, for SML and atmospheric particle samples. The variability of the FTIR composition of both atmospheric particle and SML samples is evident in the low cosine similarity values (<0.8) and high standard deviations among samples within the same type (Table 2). In contrast, seawater and gPMA samples had much more consistent FTIR spectra, shown by the high cosine similarity values (>0.93) and low standard deviations (Table 2). This range of different organic composition of SML and atmospheric aerosol samples are consistent with prior measurements showing the presence varying amounts of polymers, proteinaceous matter, and TEP in both SML and marine aerosol [*Aller et al.*, 2017; *Hendrickson et al.*, 2021; *Kuznetsova et al.*, 2005]. Longer chain saccharides have been observed to be enriched in atmospheric aerosol particles and SML that are present, but not enriched, in seawater [*Hasenecz et al.*, 2019]. The SML has been shown to have a highly heterogeneous and variable composition [*Chance et al.*, 2018; *A. Engel and Galgani*, 2016; *Zäncker et al.*, 2017], whereas seawater often has less variability [*Chance et al.*, 2018]. The IFCB cell biovolume was also more concentrated and more variable in the SML compared to the inline seawater measurements ($p<0.05$) (Figures S2 and S3). The individual particles measured by STXM-NEXAFS are also consistent with the heterogeneity of SML with particles having a range of structures from salt cores with organic coatings to solid organic to mixtures of the two.

In Figure 3, Panels C, D, and F show sampling times that have higher NPP than in Panels A, B, E (Table 1). For these days, both SML and atmospheric aerosol particle samples had higher alkane/hydroxyl ratios with high standard deviations (0.37±0.42 and 0.49±0.37, respectively), whereas seawater and gPMA samples were nearly identical with low standard deviations (0.25±0.08 and 0.08±0.04, respectively) despite the observed differences in NPP and Chl. The correlations of the four sample alkane/hydroxyl ratio to both chlorophyll (Figures S1 and S4) and NPP (Figure 5) indicate a possible role for the SML in contributing to the variability in atmospheric aerosol particle composition, perhaps driving the atmospheric particle correlation to biological tracers, as illustrated in Figure 8. The gPMA and seawater alkane-to-hydroxyl group ratio are consistently unrelated to NPP, showing almost no change for the 6 days that were sampled (0.1±0.01 (gPMA) and 0.2±0.1 (seawater) alkane/hydroxyl ratio). This could be due to gPMA and seawater organic composition being largely influenced by DOC, which is relatively invariant in concentration in comparison to POC [*Beaupré et al.*, 2019; *Frossard et al.*, 2014; *Quinn et al.*, 2014]. This smaller seawater range may contribute to the similarly small range in gPMA, suggesting that for the NAAMES open ocean conditions gPMA particles may have more contributions from seawater (and less from SML) than do the atmospheric particles. In contrast, atmospheric particles and SML samples show much wider variability, both spanning the range of 0.1 to 1 for alkane/hydroxyl ratio and showing weak positive correlations with both chlorophyll and NPP. STXM-NEXAFS showed multiple particle clusters for all sample types, however the low number of particles sampled with STXM-NEXAFS means that we cannot rule out more similarity in seawater and gPMA than in SML and atmospheric aerosol particles.

Phytoplankton blooms are associated with an increase in surface active compounds, particularly lipids, with increasing POC concentrations [*Kharbush et al.*, 2020]. Recent

contributions from bioavailable DOC [*Baetge et al.*, 2021] may explain the changing composition of the SML during these times. Atmospheric aerosol particles could also be influenced by secondary atmospheric processes of organic components, but there is no evidence of such processes changing the alkane and hydroxyl group fractions [*Frossard et al.*, 2014]. The lack of expected changes to the alkane/hydroxyl ratio from photochemical processes means that the ratio could serve as an approximately-conserved tracer for composition between these reservoirs. If this ratio is conserved on transfer between the ocean and the atmosphere, then the 0.1-1 range of alkane/hydroxyl ratio in the atmospheric particles and the SML would not be explained by the seawater source range of 0-0.3.

Similar positive correlations of alkane and hydroxyl group contributions to biological activity have also been found in gPMA aerosol particles in more productive waters, where gPMA samples had higher alkane group fractions (and lower hydroxyl group fractions) than non-productive waters during the Western Atlantic Climate Study (WACS) and California Nexus (CalNex) projects [*Frossard et al.*, 2014]. This difference from our results could be explained by the larger range of chlorophyll concentrations or the lower range of wind speeds (4 ± 2 m s^{-1} for WACS and 5 ± 2 m s^{-1} for CalNex)) in the WACS/CalNEX datasets than in NAAMES 3 and NAAMES 4. In fact, the WACS/CalNEX measurements of hydroxyl and alkane groups also did not have a clear trend for chlorophyll <1 (which is the range of all the NAAMES3 and NAAMES4 measurements), it was only at larger concentrations that the gPMA composition showed a moderate correlation to biological proxies. The contributions of SML and seawater to gPMA aerosol particles may vary with ocean conditions such as wind speed [*Obernosterer et al.*, 2008; *Rahlff et al.*, 2017], since very little is known about the prevalence and variability of the SML or its effects on gPMA sampling.

Conclusion

Our results show the organic functional groups in atmospheric particles have chemical similarities to seawater, gPMA, and SML in the North Atlantic. The four sample types were analyzed using single particle microscopy via STXM-NEXAFS and FTIR spectroscopy. Both measurements showed the presence of hydroxyl, alkyl, and alkene functional groups, and FTIR hydroxyl groups were consistently 50 - 90% of the quantified OM.

The larger range of alkane/hydroxyl group ratios, the greater FTIR spectral differences (low cosine similarity values and high standard deviations of cosine similarity values for individual spectra within the same sample type), and the weak correlations to tracers of biological activity for both atmospheric particle and SML samples suggest a biologically-influenced source contributing to a wider range of composition for SML and atmospheric particles than was found for seawater or gPMA. Both atmospheric particle and SML samples showed an increased alkane/hydroxyl ratio (associated with decreases in hydroxyl group fraction and increases in alkane group fraction) during periods of higher biological activity

tracers, which suggests that the SML was an important contributor to the organic composition of atmospheric aerosol particles. Seawater and gPMA samples had more consistent composition, showing little variation for the range of biological activity that was observed and supporting previous findings that seawater contributes a relatively invariant organic functional group composition to atmospheric aerosol particles.

Of the eight STXM-NEXAFS clusters that were identified, there were no clusters that only contained SML particle types and only one small cluster, Csalt, that was only found in a single atmospheric particle sample. This variety of particle compositions is consistent with other observations in open-ocean conditions around the world [*Hawkins and Russell*, 2010; *Russell et al.*, 2010; *G. Saliba et al.*, 2021].

The SML showed more variability in FTIR spectra among the six case-study days than either seawater or gPMA, with a FTIR cosine similarity value of 0.72 ± 0.18 for SML compared to FTIR cosine similarity values of 0.98 ± 0.02 for seawater and 0.94 ± 0.06 for gPMA. This heterogeneity of composition could explain why some reports show a robust link between marine aerosol composition and SML and others do not [*Cunliffe et al.*, 2013; *Engel et al.*, 2017; *Gasparovic et al.*, 2005; *Reinthaler et al.*, 2008; *van Pinxteren et al.*, 2017], particularly given the limited sample number of the few available studies of microlayer and aerosol composition.

The variability of the SML during sampled days displays the need for a longer time-series in which day-to-day variability can be teased apart from various environmental factors including wind speed and biological activity. Sampling the atmospheric particle and gPMA samples directly onto substrates for STXM-NEXAFS analysis would have allowed for characterization of airborne-relevant particle morphology and diameter, and additional sampling would have provided a more robust data set for understanding seasonal and regional differences.

Acknowledgements. This is PMEL contribution number 5369.

References:

Aller, J. Y., M. R. Kuznetsova, C. J. Jahns, and P. F. Kemp (2005), The sea surface microlayer as a source of viral and bacterial enrichment in marine aerosols, *Journal of Aerosol Science*, *36*(5), 801-812, doi:https://doi.org/10.1016/j.jaerosci.2004.10.012.

Aller, J. Y., J. C. Radway, W. P. Kilthau, D. W. Bothe, T. W. Wilson, R. D. Vaillancourt, P. K. Quinn, D. J. Coffman, B. J. Murray, and D. A. Knopf (2017), Size-resolved characterization of the polysaccharidic and proteinaceous components of sea spray aerosol, *Atmospheric Environment*, *154*, 331-347, doi:https://doi.org/10.1016/j.atmosenv.2017.01.053.

Baetge, N., M. J. Behrenfeld, J. Fox, K. H. Halsey, K. D. A. Mojica, A. Novoa, B. M. Stephens, and C. A. Carlson (2021), The Seasonal Flux and Fate of Dissolved Organic Carbon Through Bacterioplankton in the Western North Atlantic, *Frontiers in Microbiology*, *12*, doi:10.3389/fmicb.2021.669883.

Bao, H., J. Niggemann, L. Luo, T. Dittmar, and S.-J. Kao (2017), Aerosols as a source of dissolved black carbon to the ocean, *Nature Communications*, *8*(1), doi:10.1038/s41467-017-00437-3.

Bates, T. S., P. K. Quinn, D. J. Coffman, J. E. Johnson, L. Upchurch, G. Saliba, S. Lewis, J. Graff, L. M. Russell, and M. J. Behrenfeld (2020), Variability in Marine Plankton Ecosystems Are Not Observed in Freshly Emitted Sea Spray Aerosol Over the North Atlantic Ocean, *Geophysical Research Letters*, *47*(1), e2019GL085938, doi:10.1029/2019GL085938.
Bates, T. S., et al. (2012), Measurements of ocean derived aerosol off the coast of California, *Journal of Geophysical Research-Atmospheres*, *117*, doi:10.1029/2012jd017588.
Beaupré, S. R., et al. (2019), Oceanic efflux of ancient marine dissolved organic carbon in primary marine aerosol, *Science Advances*, *5*(10), eaax6535, doi:10.1126/sciadv.aax6535.
Behrenfeld, M. J., et al. (2019), The North Atlantic Aerosol and Marine Ecosystem Study (NAAMES): Science Motive and Mission Overview, *Frontiers in Marine Science*, *6*(122), doi:10.3389/fmars.2019.00122.
Blanchard, D. C. (1964), Sea-to-Air Transport of Surface Active Material, *Science*, *146*(3642), 396, doi:10.1126/science.146.3642.396.
Boss, E., M. Twardowski, and S. Herring (2001), Shape of the particulate beam attenuation spectrum and its inversion to obtainthe shape of the particulate size distribution, *Appl. Opt.*, *40*(27), 4885--4893, doi:10.1364/AO.40.004885.
Carlson, C. A., and D. A. Hansell (2015), Chapter 3 - DOM Sources, Sinks, Reactivity, and Budgets, in *Biogeochemistry of Marine Dissolved Organic Matter (Second Edition)*, edited by D. A. Hansell and C. A. Carlson, pp. 65-126, Academic Press, Boston, doi:https://doi.org/10.1016/B978-0-12-405940-5.00003-0.
Carlson, D. J., and L. M. Mayer (1980), Enrichment of dissolved phenolic material in the surface microlayer of coastal waters, *Nature*, *286*(5772), 482-483, doi:10.1038/286482a0.
Cetinić, I., M. J. Perry, N. T. Briggs, E. Kallin, E. A. D'Asaro, and C. M. Lee (2012), Particulate organic carbon and inherent optical properties during 2008 North Atlantic Bloom Experiment, *Journal of Geophysical Research: Oceans*, *117*(C6), doi:https://doi.org/10.1029/2011JC007771.
Chance, R. J., J. F. Hamilton, L. J. Carpenter, S. C. Hackenberg, S. J. Andrews, and T. W. Wilson (2018), Water-Soluble Organic Composition of the Arctic Sea Surface Microlayer and Association with Ice Nucleation Ability, *Environmental Science & Technology*, *52*(4), 1817-1826, doi:10.1021/acs.est.7b04072.
Chase, A. P., S. J. Kramer, N. Haëntjens, E. S. Boss, L. Karp-Boss, M. Edmondson, and J. R. Graff (2020), Evaluation of diagnostic pigments to estimate phytoplankton size classes, *Limnology and Oceanography: Methods*, *18*(10), 570-584, doi:10.1002/lom3.10385.
Crilley, L. R., G. A. Ayoko, and L. Morawska (2013), Analysis of organic aerosols collected on filters by Aerosol Mass Spectrometry for source identification, *Analytica Chimica Acta*, *803*, 91-96, doi:https://doi.org/10.1016/j.aca.2013.07.013.
Cunliffe, M., A. Engel, S. Frka, B. Gašparović, C. Guitart, J. C. Murrell, M. Salter, C. Stolle, R. Upstill-Goddard, and O. Wurl (2013), Sea surface microlayers: A unified physicochemical and biological perspective of the air–ocean interface, *Progress in Oceanography*, *109*, 104-116, doi:https://doi.org/10.1016/j.pocean.2012.08.004.
Cunliffe, M., and O. Wurl (2014), Guide to best practices to study the ocean's surface, 19 - 31, doi:10.25607/OBP-1512.
Drozdowska, V., I. Wrobel, P. Markuszewski, P. Makuch, A. Raczkowska, and P. Kowalczuk (2017), Study on organic matter fractions in the surface microlayer in the Baltic Sea by spectrophotometric and spectrofluorometric methods, *Ocean Science*, *13*(5), 633-647, doi:10.5194/os-13-633-2017.
Engel, A., et al. (2017), The Ocean's Vital Skin: Toward an Integrated Understanding of the Sea Surface Microlayer, *Frontiers in Marine Science*, *4*(165), doi:10.3389/fmars.2017.00165.
Engel, A., and L. Galgani (2016), The organic sea-surface microlayer in the upwelling region off the coast of Peru and potential implications for air–sea exchange processes, *Biogeosciences*, *13*(4), 989-1007, doi:10.5194/bg-13-989-2016.

Facchini, M. C., et al. (2008), Primary submicron marine aerosol dominated by insoluble organic colloids and aggregates, *Geophysical Research Letters*, *35*(17), doi:https://doi.org/10.1029/2008GL034210.
Fox, J., et al. (2020), Phytoplankton Growth and Productivity in the Western North Atlantic: Observations of Regional Variability From the NAAMES Field Campaigns, *Frontiers in Marine Science*, *7*(24), doi:10.3389/fmars.2020.00024.
Frossard, A. A., and L. M. Russell (2012), Removal of Sea Salt Hydrate Water from Seawater-Derived Samples by Dehydration, *Environmental Science & Technology*, *46*(24), 13326-13333, doi:10.1021/es3032083.
Frossard, A. A., L. M. Russell, S. M. Burrows, S. M. Elliott, T. S. Bates, and P. K. Quinn (2014), Sources and composition of submicron organic mass in marine aerosol particles, *Journal of Geophysical Research: Atmospheres*, *119*(22), 12,977-913,003, doi:10.1002/2014JD021913.
Gagosian, R. B., and D. H. Stuermer (1977), The cycling of biogenic compounds and their diagenetically transformed products in seawater, *Marine Chemistry*, *5*(4), 605-632, doi:https://doi.org/10.1016/0304-4203(77)90045-7.
Garrett, W. D. (1967), The organic chemical composition of the ocean surface, *Deep Sea Research and Oceanographic Abstracts*, *14*(2), 221-227, doi:https://doi.org/10.1016/0011-7471(67)90007-1.
Gasparovic, B., M. Plavšić, B. Ćosović, and M. Reigstad (2005), Organic matter characterization and fate in the sub-arctic Norwegian fjords during the late spring/summer period, *Estuarine, Coastal and Shelf Science*, *62*, 95-107, doi:10.1016/j.ecss.2004.08.008.
Hansell, D. A., C. A. Carlson, D. J. Repeta, and R. Schlitzer (2009), DISSOLVED ORGANIC MATTER IN THE OCEAN

A CONTROVERSY STIMULATES NEW INSIGHTS, *Oceanography*, *22*(4), 202-211.
Hasenecz, E. S., C. P. Kaluarachchi, H. D. Lee, A. V. Tivanski, and E. A. Stone (2019), Saccharide Transfer to Sea Spray Aerosol Enhanced by Surface Activity, Calcium, and Protein Interactions, *ACS Earth and Space Chemistry*, *3*(11), 2539-2548, doi:10.1021/acsearthspacechem.9b00197.
Hawkins, L. N., and L. M. Russell (2010), Polysaccharides, Proteins, and Phytoplankton Fragments: Four Chemically Distinct Types of Marine Primary Organic Aerosol Classified by Single Particle Spectromicroscopy, *Advances in Meteorology*, *2010*, 14, doi:10.1155/2010/612132.
Hayase, K., and H. Tsubota (1983), Sedimentary humic acid and fulvic acid as surface active substances, *Geochimica et Cosmochimica Acta*, *47*(5), 947-952, doi:https://doi.org/10.1016/0016-7037(83)90160-6.
Hendrickson, B. N., S. D. Brooks, D. C. O. Thornton, R. H. Moore, E. Crosbie, L. D. Ziemba, C. A. Carlson, N. Baetge, J. A. Mirrielees, and A. N. Alsante (2021), Role of Sea Surface Microlayer Properties in Cloud Formation, *Frontiers in Marine Science*, *7*, doi:10.3389/fmars.2020.596225.
Hunter, K. A., and P. S. Liss (1977), The input of organic material to the oceans: air—sea interactions and the organic chemical composition of the sea surface, *Marine Chemistry*, *5*(4), 361-379, doi:https://doi.org/10.1016/0304-4203(77)90029-9.
Kharbush, J. J., et al. (2020), Particulate Organic Carbon Deconstructed: Molecular and Chemical Composition of Particulate Organic Carbon in the Ocean, *Frontiers in Marine Science*, *7*, doi:10.3389/fmars.2020.00518.
Knulst, J. C., R. C. Boerschke, and S. Loemo (1998), Differences in Organic Surface Microlayers from an Artificially Acidified and Control Lake, Elucidated by XAD-8/XAD-4 Tandem Separation and Solid State 13C NMR Spectroscopy, *Environmental Science & Technology*, *32*(1), 8-12, doi:10.1021/es9609819.
Kuznetsova, M., C. Lee, and J. Aller (2005), Characterization of the proteinaceous matter in marine aerosols, *Marine Chemistry*, *96*(3), 359-377, doi:https://doi.org/10.1016/j.marchem.2005.03.007.
Laskin, A., R. C. Moffet, M. K. Gilles, J. D. Fast, R. A. Zaveri, B. Wang, P. Nigge, and J. Shutthanandan (2012), Tropospheric chemistry of internally mixed sea salt and organic particles: Surprising reactivity of

NaCl with weak organic acids, *Journal of Geophysical Research: Atmospheres*, *117*(D15), doi:https://doi.org/10.1029/2012JD017743.
Lewis, S. L., G. Saliba, L. M. Russell, P. K. Quinn, T. S. Bates, and M. J. Behrenfeld (2021), Seasonal Differences in Submicron Marine Aerosol Particle Organic Composition in the North Atlantic, *Frontiers in Marine Science*, *8*, doi:10.3389/fmars.2021.720208.
Liss, P., and Duce, R. (1997), *The Sea Surface and Global Change*, Cambridge University Press, Cambridge, doi:DOI: 10.1017/CBO9780511525025.
Maria, S. F., L. M. Russell, B. J. Turpin, and R. J. Porcja (2002), FTIR measurements of functional groups and organic mass in aerosol samples over the Caribbean, *Atmospheric Environment*, *36*(33), 5185-5196, doi:10.1016/s1352-2310(02)00654-4.
Maria Steven, F., M. Russell Lynn, K. Gilles Mary, and C. B. Myneni Satish (2004), Organic Aerosol Growth Mechanisms and Their Climate-Forcing Implications, *Science*, *306*(5703), 1921-1924, doi:10.1126/science.1103491.
Moberg, E. A., and H. M. Sosik (2012), Distance maps to estimate cell volume from two-dimensional plankton images, *Limnology and Oceanography: Methods*, *10*(4), 278-288, doi:10.4319/lom.2012.10.278.
Obernosterer, I., P. Catala, R. Lami, J. Caparros, J. Ras, A. Bricaud, C. Dupuy, F. van Wambeke, and P. Lebaron (2008), Biochemical characteristics and bacterial community structure of the sea surface microlayer in the South Pacific Ocean, *Biogeosciences*, *5*(3), 693-705, doi:10.5194/bg-5-693-2008.
Quinn, P. K., T. S. Bates, K. S. Schulz, D. J. Coffman, A. A. Frossard, L. M. Russell, W. C. Keene, and D. J. Kieber (2014), Contribution of sea surface carbon pool to organic matter enrichment in sea spray aerosol, *Nature Geoscience*, *7*(3), 228-232, doi:10.1038/ngeo2092.
Rahlff, J., C. Stolle, H.-A. Giebel, T. Brinkhoff, M. Ribas-Ribas, D. Hodapp, and O. Wurl (2017), High wind speeds prevent formation of a distinct bacterioneuston community in the sea-surface microlayer, *FEMS microbiology ecology*, *93*(5), fix041, doi:10.1093/femsec/fix041.
Reinthaler, T., E. Sintes, and G. J. Herndl (2008), Dissolved organic matter and bacterial production and respiration in the sea-surface microlayer of the open Atlantic and the western Mediterranean Sea, *Limnology and Oceanography*, *53*(1), 122-136, doi:https://doi.org/10.4319/lo.2008.53.1.0122.
Russell, L. M. (2003), Aerosol Organic-Mass-to-Organic-Carbon Ratio Measurements, *Environmental Science & Technology*, *37*(13), 2982-2987, doi:10.1021/es026123w.
Russell, L. M., R. Bahadur, L. N. Hawkins, J. Allan, D. Baumgardner, P. K. Quinn, and T. S. Bates (2009a), Organic aerosol characterization by complementary measurements of chemical bonds and molecular fragments, *Atmospheric Environment*, *43*(38), 6100-6105, doi:10.1016/j.atmosenv.2009.09.036.
Russell, L. M., L. N. Hawkins, A. A. Frossard, P. K. Quinn, and T. S. Bates (2010), Carbohydrate-like composition of submicron atmospheric particles and their production from ocean bubble bursting, *Proceedings of the National Academy of Sciences of the United States of America*, *107*(15), 6652-6657, doi:10.1073/pnas.0908905107.
Russell, L. M., S. F. Maria, and S. C. B. Myneni (2002), Mapping organic coatings on atmospheric particles, *Geophysical Research Letters*, *29*(16), 26-21-26-24, doi:https://doi.org/10.1029/2002GL014874.
Russell, L. M., S. Takahama, S. Liu, L. N. Hawkins, D. S. Covert, P. K. Quinn, and T. S. Bates (2009b), Oxygenated fraction and mass of organic aerosol from direct emission and atmospheric processing measured on the R/V Ronald Brown during TEXAQS/GoMACCS 2006, *Journal of Geophysical Research: Atmospheres*, *114*(D7), doi:10.1029/2008jd011275.
Saliba, G., et al. (2020), Seasonal Differences and Variability of Concentrations, Chemical Composition, and Cloud Condensation Nuclei of Marine Aerosol Over the North Atlantic, *Journal of Geophysical Research: Atmospheres*, *125*(19), e2020JD033145, doi:10.1029/2020JD033145.

Saliba, G., et al. (2021), Organic composition of three different size ranges of aerosol particles over the Southern Ocean, *Aerosol Science and Technology*, *55*(3), 268-288, doi:10.1080/02786826.2020.1845296.
Takahama, S., S. Gilardoni, L. M. Russell, and A. L. D. Kilcoyne (2007), Classification of multiple types of organic carbon composition in atmospheric particles by scanning transmission X-ray microscopy analysis, *Atmospheric Environment*, *41*(40), 9435-9451, doi:10.1016/j.atmosenv.2007.08.051.
Takahama, S., A. Johnson, and L. M. Russell (2013), Quantification of Carboxylic and Carbonyl Functional Groups in Organic Aerosol Infrared Absorbance Spectra, *Aerosol Science and Technology*, *47*(3), 310-325, doi:10.1080/02786826.2012.752065.
Takahama, S., S. Liu, and L. M. Russell (2010), Coatings and clusters of carboxylic acids in carbon-containing atmospheric particles from spectromicroscopy and their implications for cloud-nucleating and optical properties, *Journal of Geophysical Research-Atmospheres*, *115*(D01202), doi:10.1029/2009jd012622.
Tseng, R.-S., J. T. Viechnicki, R. A. Skop, and J. W. Brown (1992), Sea-to-air transfer of surface-active organic compounds by bursting bubbles, *Journal of Geophysical Research: Oceans*, *97*(C4), 5201-5206, doi:https://doi.org/10.1029/91JC00954.
van Pinxteren, M., S. Barthel, K. W. Fomba, K. Müller, W. von Tümpling, and H. Herrmann (2017), The influence of environmental drivers on the enrichment of organic carbon in the sea surface microlayer and in submicron aerosol particles – measurements from the Atlantic Ocean, *Elementa: Science of the Anthropocene*, *5*, doi:10.1525/elementa.225.
Vedrinskii, R. V., L. A. Bugaev, I. I. Gegusin, V. L. Kraizman, A. A. Novakovich, S. A. Prosandeev, R. E. Ruus, A. A. Maiste, and M. A. Elango (1982), X-ray absorption near edge structure (XANES) for KCl, *Solid State Communications*, *44*(10), 1401-1407, doi:https://doi.org/10.1016/0038-1098(82)90019-9.
Wurl, O., and M. Holmes (2008), The gelatinous nature of the sea-surface microlayer, *Marine Chemistry*, *110*(1), 89-97, doi:https://doi.org/10.1016/j.marchem.2008.02.009.
Zäncker, B., A. Bracher, R. Röttgers, and A. Engel (2017), Variations of the Organic Matter Composition in the Sea Surface Microlayer: A Comparison between Open Ocean, Coastal, and Upwelling Sites Off the Peruvian Coast, *Frontiers in Microbiology*, *8*(2369), doi:10.3389/fmicb.2017.02369.

Tables:

Table 1 – Concurrent sampling times and station information including latitude, longitude, wind speeds, chlorophyll concentrations, NPP rates, seawater temperatures, number of above detection filters of the four sample sources for FTIR, and the number of above detection particles, averaged per sample source, for STXM-NEXAFS with the number of particles within the average in parenthesis.

Date	Station	Lat(°)	Long (°)	Wind Speed (ms^{-1})	Chl-A (5 m, $\mu g\ L^{-1}$)	NPP ($\mu mol\ C\ L^{-1}d^{-1}$)	SW temp (°C)	FTIR ADL samples	STXM-NEXAFS ADL samples
9/10/2017	N3 S4	48	39	6.5	0.23	0.19	16.8	3	3 (13)
9/12/2017	N3 S5	51	39	5.8	0.31	0.42	14.3	4	4 (13)
9/15/ 2017	N3 S6	53	39	5.7	0.79	0.59	11.7	3	3 (22)
9/16/2017	N3 S6	53	39	7.3	0.83	0.72	11.7	2	2 (12)
3/27/2018	N4 S1	39	43	10.2	0.85	0.60	18.8	3	3 (18)
4/3/2018	N4 S2-RD	40	39	10.4	0.72	1.31	17.9	4	4 (17)

Table 2 – Cosine similarity values with the standard deviation of the 4 different sources (Atmospheric particles (Atm), sea surface microlayer (SML), generated primary marine aerosol (gPMA), and seawater (SW)) between both STXM and FTIR spectra.

	Average STXM-NEXAFS Cosine Similarity				Average FTIR Cosine Similarity			
	Atm	**SML**	**gPMA**	**SW**	**Atm**	**SML**	gPMA	**SW**
Atm	0.95±0.10	-	-	-	0.75±0.15	-	-	-
SML	0.97±0.02	0.98±0.02	-	-	0.73±0.16	0.72±0.18	-	-
SS	0.97±0.02	0.97±0.02	0.97±0.02	-	0.76±0.17	0.78±0.15	0.94±0.06	-
SW	0.97±0.02	0.98±0.02	0.97±0.02	0.97±0.02	0.83±0.06	0.85±0.08	0.88±0.05	0.98±0.02

Table 3 – Summary of clustered particle types with the cosine similarity between the literature clusters ([*G. Saliba et al.*, 2021; *S. Takahama et al.*, 2007] and the clusters derived from k-means clustering in this study. The number of functional group peaks shared between the literature clusters and the clusters of this study (common peaks), the number of particles within each cluster, and the number of particles within the cluster separated by sample type are displayed.

Category	Cosine Similarity	Common peaks	N	Seawater	SML	gPMA	Atmospheric
d	0.99	1	17	0	4	3	10
g	0.96	2	9	1	4	1	3
j	0.94	4	24	0	13	4	7
l	0.99	2	10	2	7	0	1
m	0.99	2	13	2	4	3	4
Macid	0.95	4	25	2	6	4	13
Mcarb	0.98	3	21	0	0	4	17
Csalt	-	-	3	0	0	0	3

Figures:

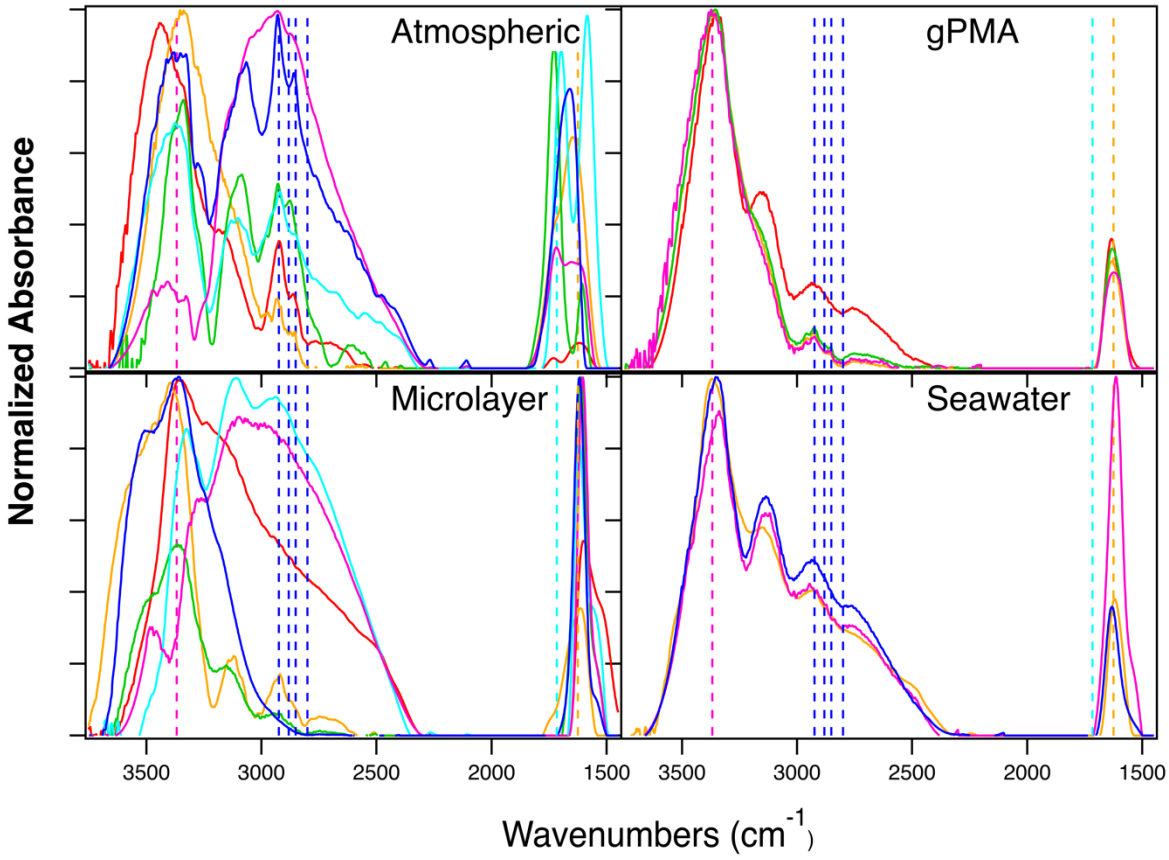

Figure 1: Normalized FTIR spectra from 4 sample types (Atmospheric, gPMA, Microlayer, and Seawater) collected on 6 different days: 09/10/17 (red), 09/12/17 (orange), 09/15/17 (green), 09/16/17 (teal), 03/27/18 (blue), and 04/03/18 (pink). The dashed vertical lines indicate the hydroxyl group peak location at 3369 cm^{-1} (pink), alkane group peak locations at 2800, 2852, 2882, and 2925 cm^{-1} (blue lines), carbonyl group peak location at 1717 cm^{-1} (teal), and amine group peak location at 1625 cm^{-1} (orange).

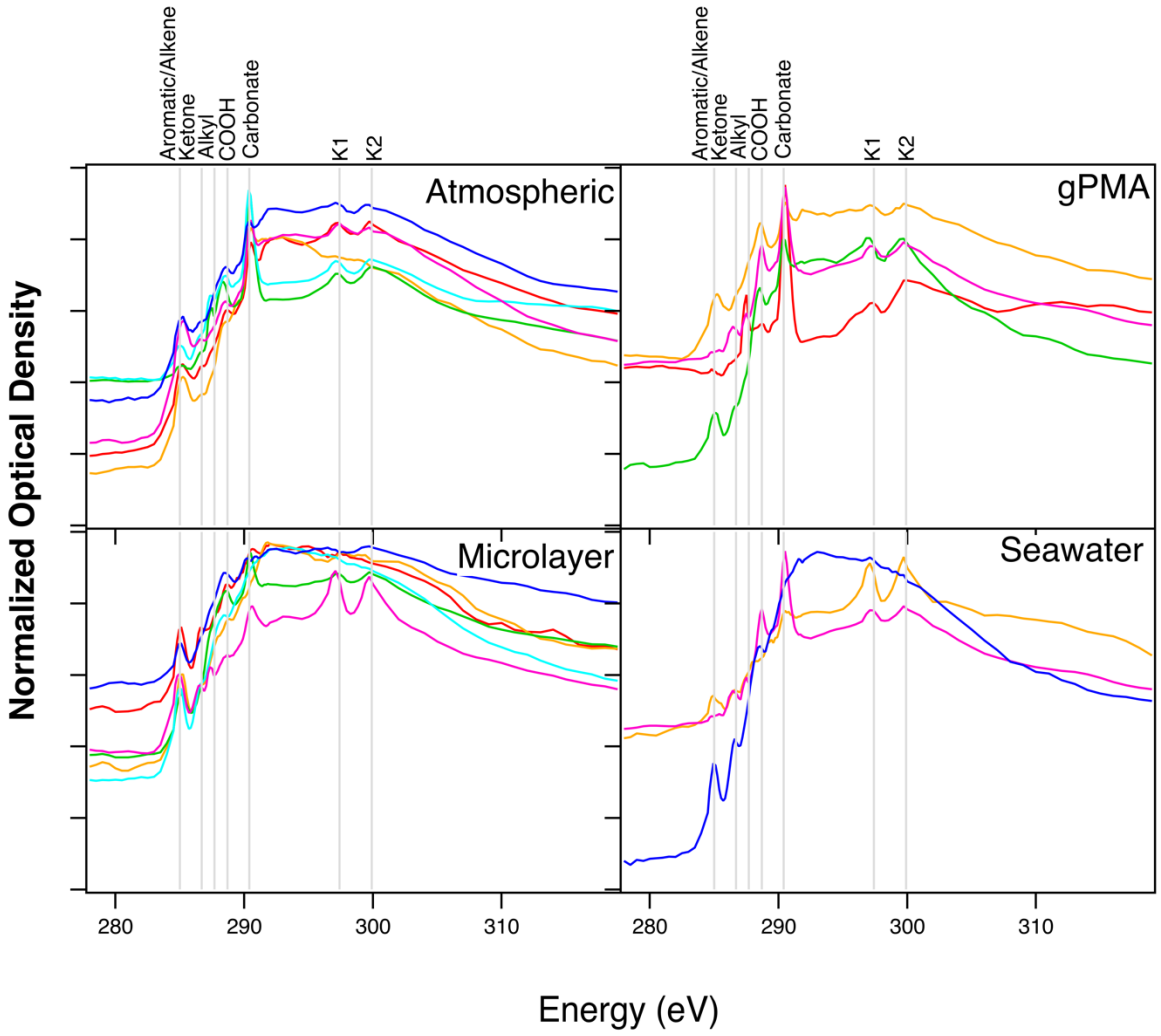

Figure 2: Normalized STXM-NEXAFS centroids from 4 sample types (Atmospheric, gPMA, Microlayer, and Seawater) collected on 6 different days: 09/10/17 (red), 09/12/17 (orange), 09/15/17 (green), 09/16/17 (teal), 03/27/18 (blue), and 04/03/18 (pink). Vertical grey lines in each panel indicate peak locations for the selected functional groups, from left to right, are aromatic (285 eV), ketone (286.7 eV), alkyl (287.7 eV), carboxylic acid (288.7 eV), carbonate (290.4 eV), and two potassium peaks (297.4 and 299.9 eV).

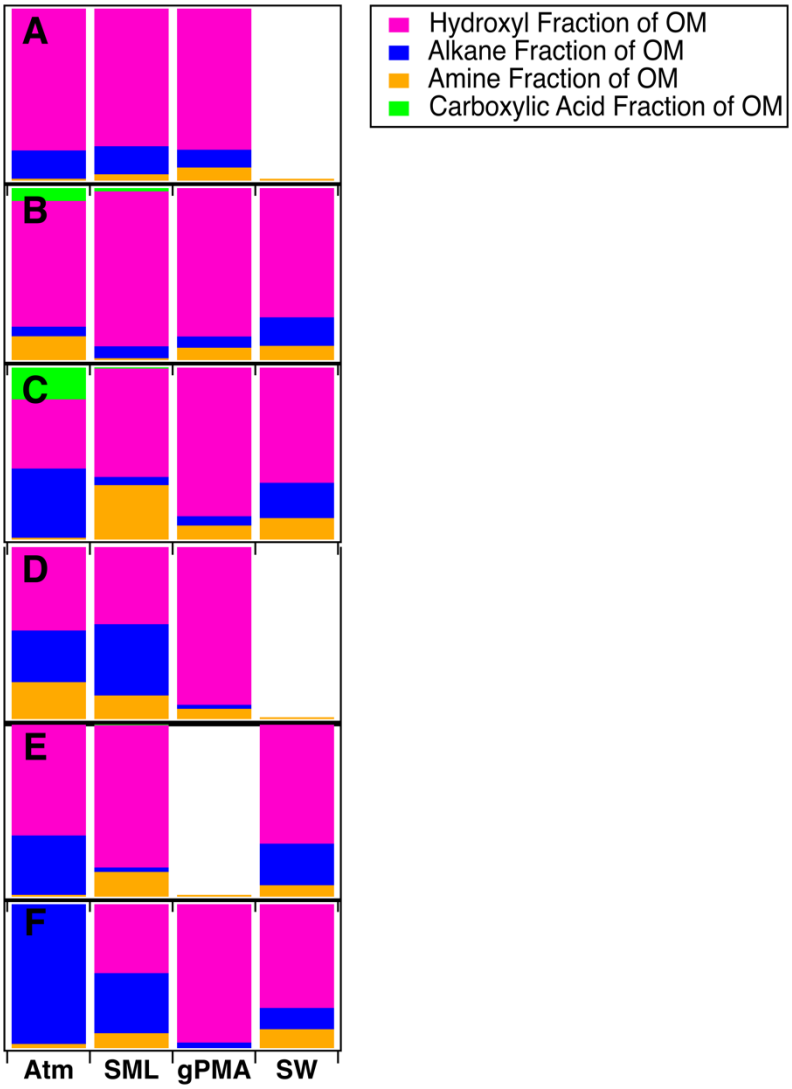

Figure 3: The organic functional group fraction from FTIR spectra with hydroxyl groups (pink), alkane groups (blue), amine groups (orange), and acid groups (green). The four sample types are atmospheric particles (Atm), sea surface microlayer (SML), gPMA, and seawater (SW). The panels show the dates sampled: (A) 09/10/17, (B) 09/12/17, (C) 09/15/17, (D) 09/16/17, (E) 03/27/18, and (F) 04/03/18. The seasonal change occurs between panels D and E and is denoted with a thick black bar.

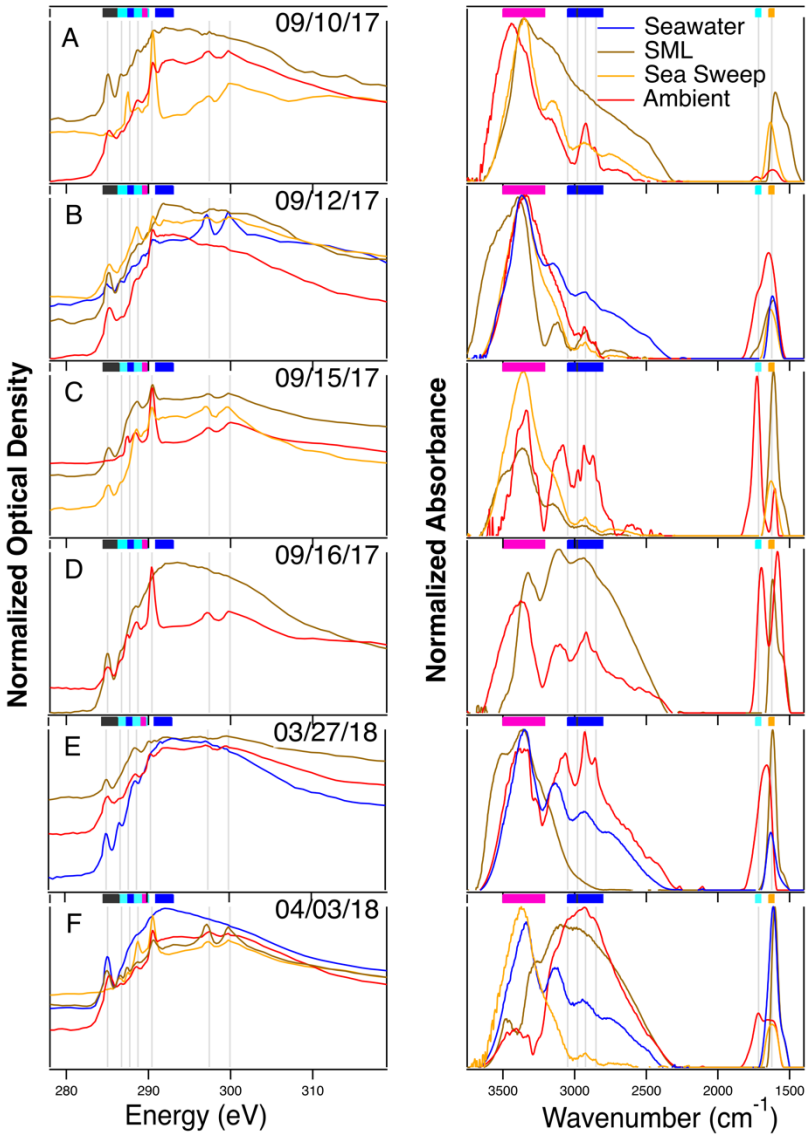

Figure 4: Sample averaged normalized STXM-NEXAFS spectra from 6 separate days (left column) and normalized FTIR spectra (right column). Spectra were normalized to the highest absorbance peak before averaging. The rows show the dates sampled: (A) 09/10/17, (B) 09/12/17, (C) 09/15/17, (D) 09/16/17, (E) 03/27/18, and (F) 04/03/18. The colored bars on top indicate shared functional group peak locations with aromatic/alkene absorption in black, hydroxyl in pink, alkane in blue, carbonyl in teal, and amine in orange. The STXM-NEXAFS functional groups identified by the grey lines, from left to right, are aromatic (285 eV), ketone (286.7 eV), alkyl (287.7 eV), carboxylic acid (288.7 eV), carbonate (290.4 eV), and two potassium peaks (297.4 and 299.9 eV).

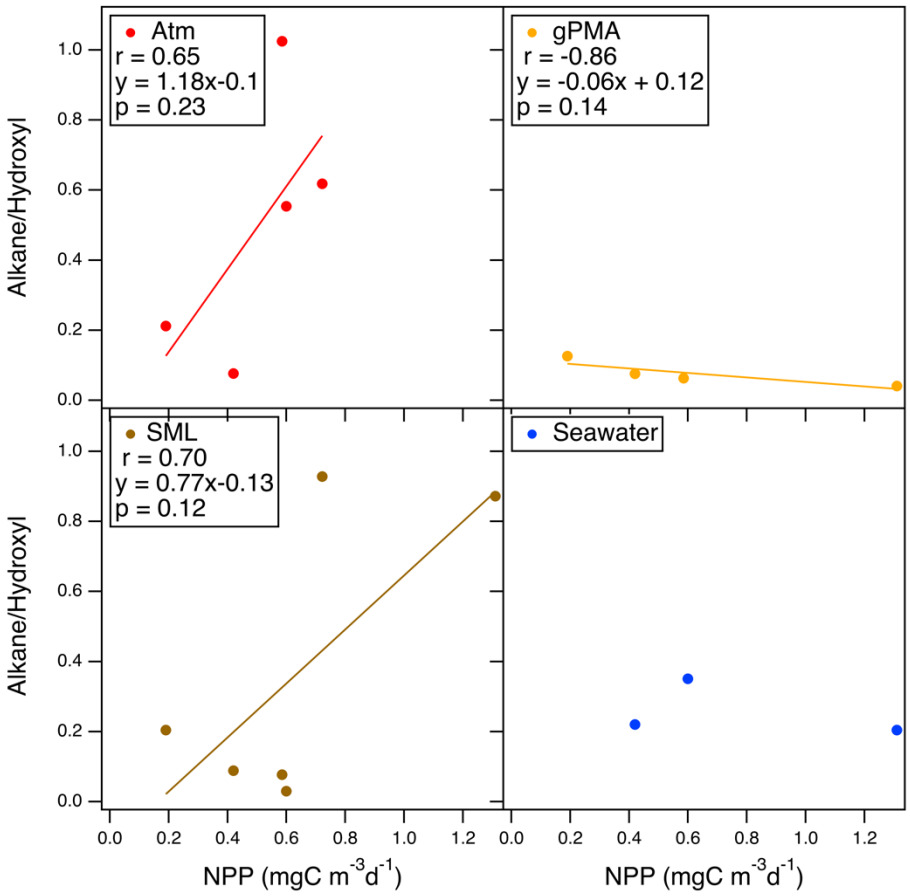

.

Figure 5: The alkane to hydroxyl ratio of atmospheric particle (top left), SML (bottom left), gPMA (top right), and seawater (bottom right) samples compared to NPP. NPP was integrated and normalized to the depth of the euphotic zone and obtained from [*Baetge et al.*, 2021]. Linear fit lines are shown for r>0.3. The points include measurements above detection for sample types collected on 09/10/17, 09/12/17, 09/15/17, 09/16/17, 03/27/18, and 04/03/18.

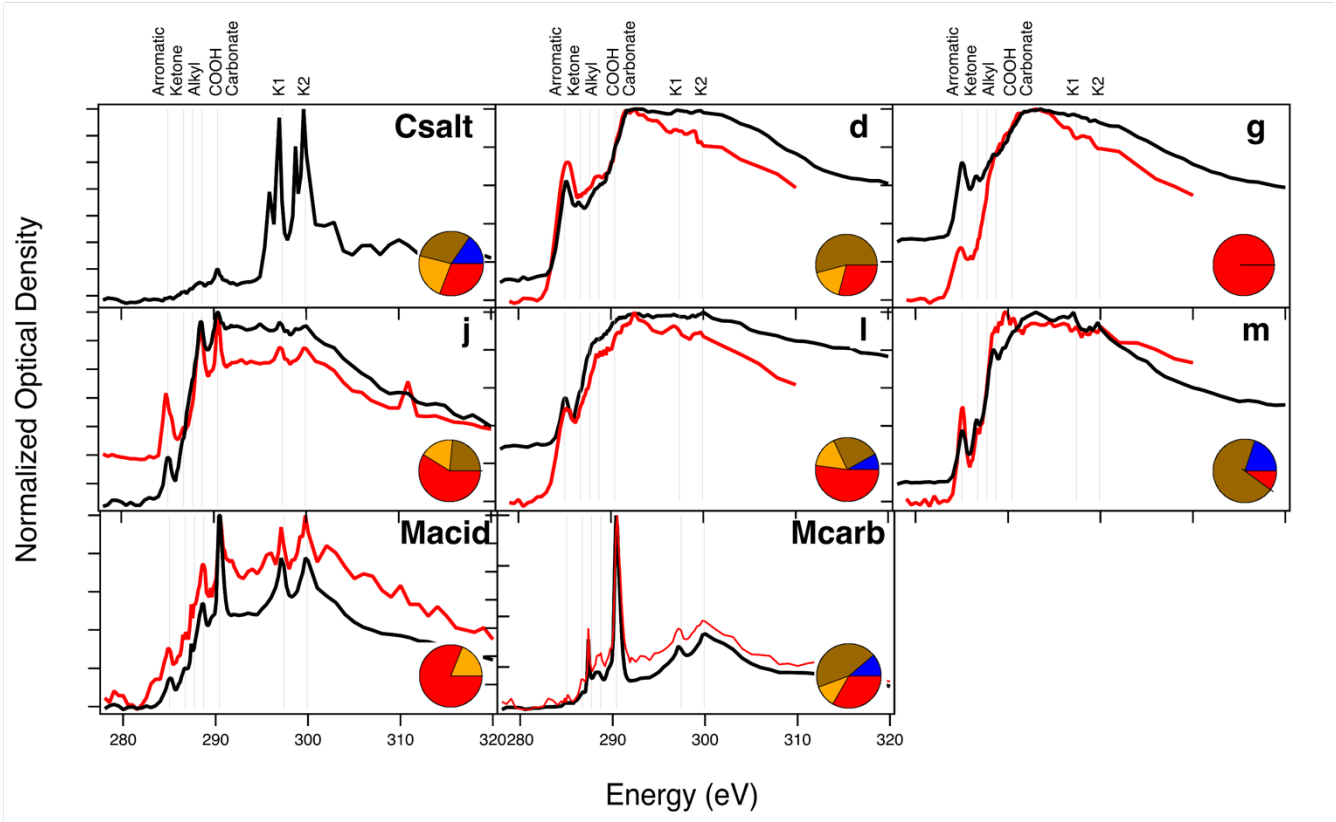

Figure 6: Normalized k-means STXM-NEXAFS clusters from the NAAMES campaign (black) compared to reference STXM-NEXAFS spectra (red). The reference spectra in m, j, d, l, and g are from Takahama et al. [2007] and the reference spectra from Macid and Mcarb are from Saliba et al. [2021]. Vertical grey lines in each panel indicate peak locations for the selected functional groups, from left to right, are aromatic (285 eV), ketone (286.7 eV), alkyl (287.7 eV), carboxylic acid (288.7 eV), carbonate (290.4 eV), and two potassium peaks (297.4 and 299.9 eV). The pie chart indicates the number of particles from each sample type with seawater in blue, SML in brown, gPMA in orange, and atmospheric particle in red.

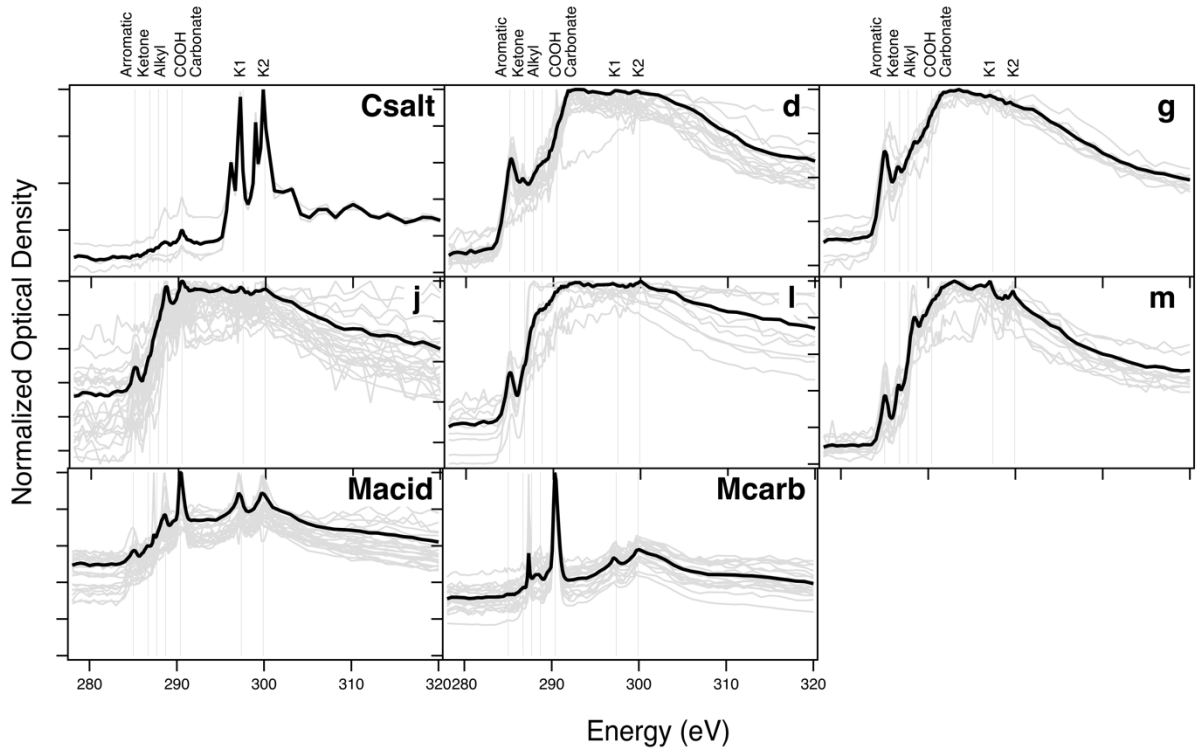

Figure 7: Normalized k-means cluster centroids of STXM-NEXAFS spectra from NAAMES campaign (black) and the individual particle-averaged STXM-NEXAFS spectra that comprise each cluster (grey). Reference spectra labeling is the same as Figure 6. Vertical grey lines in each panel indicate peak locations for the selected functional groups, from left to right, are aromatic (285 eV), ketone (286.7 eV), alkyl (287.7 eV), carboxylic acid (288.7 eV), carbonate (290.4 eV), and two potassium peaks (297.4 and 299.9 eV).

.

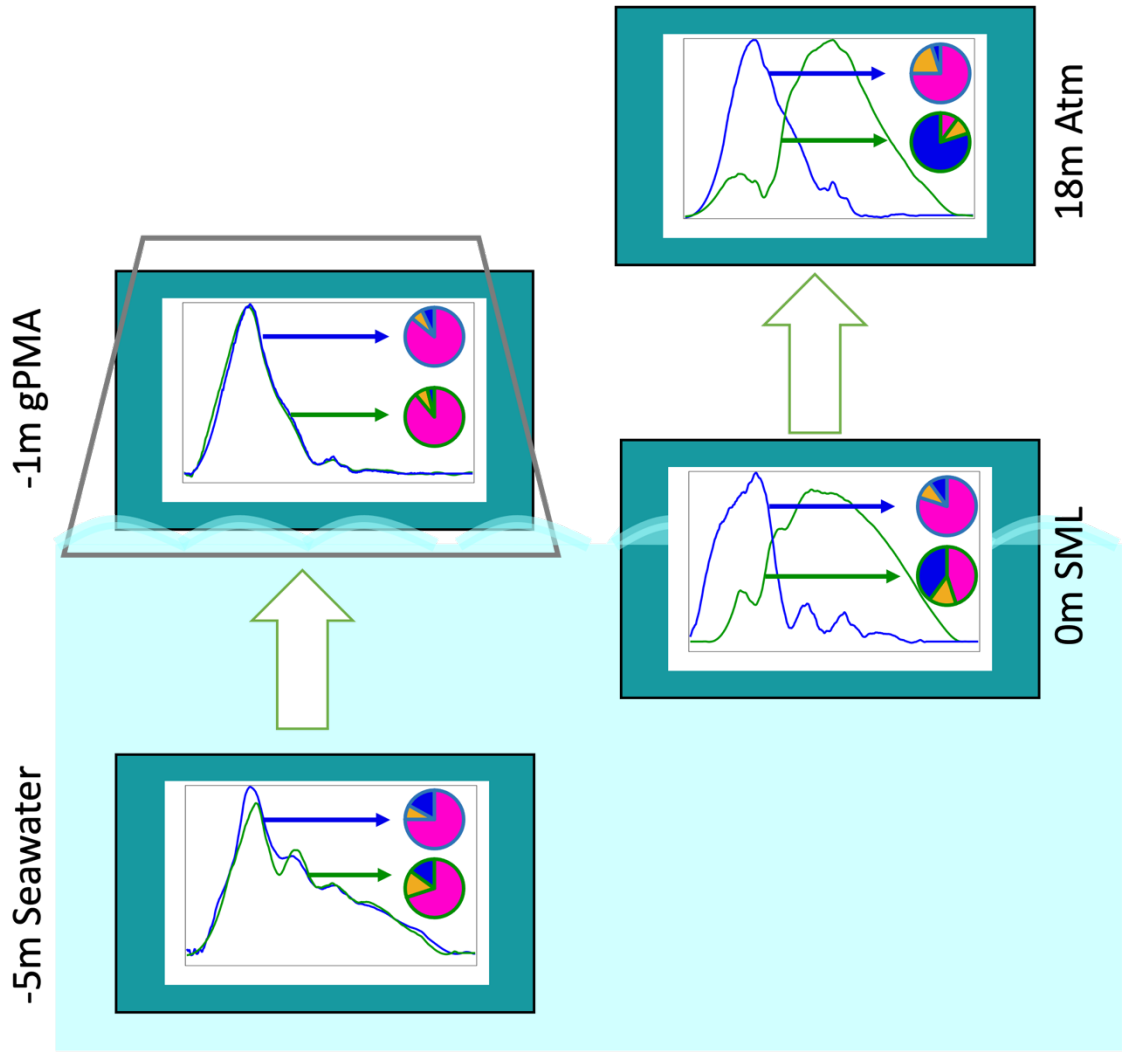

Figure 8: Diagram illustrating the influence of seawater (bottom left) on gPMA (top left with a trapezoid representing Sea Sweep) aerosol particle composition and the influence of SML (bottom right) on atmospheric particle composition (top right). The arrows are based on the similarity of composition shown in the pie charts and the spectra and do not indicate that they are the only source as seawater and SML components can be mixed. The FTIR spectra shown are during a lower chlorophyll period (blue, 12 September 2017) and higher chlorophyll period (green, 3 April 2018). The pie graphs, outlined in corresponding color for low vs. high chlorophyll demonstrate the organic functional group FTIR composition with hydroxyl groups (pink), alkane groups (blue), and amine groups (orange).